analytical chemistry

Article

pubs.acs.org/ac

Microfluidic System for In-Flow Reversible Photoswitching of Near-Infrared Fluorescent Proteins

Vladislav V. Lychagov,[†,‡] Anton A. Shemetov,[†,‡] Ralph Jimenez,[*,§,∥] and Vladislav V. Verkhusha[*,†,‡,⊥]

[†]Department of Anatomy and Structural Biology and [‡]Gruss-Lipper Biophotonics Center, Albert Einstein College of Medicine, Bronx, New York 10461, United States

[§]JILA, National Institute of Standards and Technology and [∥]Department of Chemistry and Biochemistry, University of Colorado, Boulder, Colorado 80309, United States

[⊥]Department of Biochemistry and Developmental Biology, Faculty of Medicine, University of Helsinki, Helsinki 00029, Finland

Supporting Information

ABSTRACT: We have developed a microfluidic flow cytometry system to screen reversibly photoswitchable fluorescent proteins for contrast and stability of reversible photoconversion between high- and low-fluorescent states. A two-color array of 20 excitation and deactivation beams generated with diffractive optics was combined with a serpentine microfluidic channel geometry designed to provide five cycles of photoswitching with real-time calculation of photoconversion fluorescence contrast. The characteristics of photoswitching in-flow as a function of excitation and deactivation beam fluence, flow speed, and protein concentration were studied with droplets of the bacterial phytochrome from *Deinococcus radiodurans* (DrBphP), which is weakly fluorescent in the near-infrared (NIR) spectral range. In agreement with measurements on stationary droplets and HeLa S3 mammalian cells expressing DrBphP, optimized operation of the flow system provided up to 50% photoconversion contrast in-flow at a droplet rate of few hertz and a coefficient of variation (CV) of up to 2% over 10 000 events. The methods for calibrating the brightness and photoswitching measurements in microfluidic flow established here provide a basis for screening of cell-based libraries of reversibly switchable NIR fluorescent proteins.

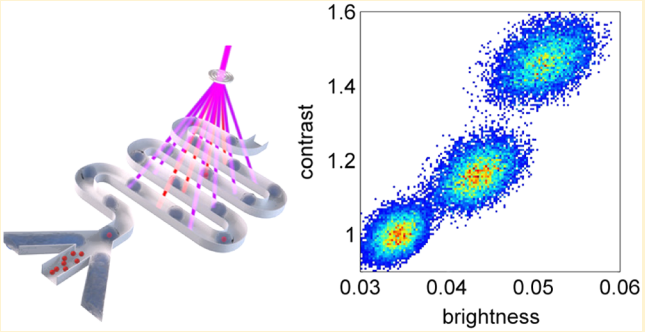

Since its invention in the 1990s, fluorescence microscopy-based super-resolution imaging techniques[1−4] have been developed by many groups and have found their place in numerous applications. These advances have been reviewed recently.[5−7] Regardless of the particular technique (pointwise scanning with shaped beams in STED/GSD[1,2,8] or stochastic excitation/emission under full-field illumination in STORM/PALM[9,10]), characteristics of the fluorescent probes critically influence imaging performance.[7,11−13] The importance of the photophysical factors for required fluorescent probes were first recognized in a generalization of STED − scanning GSD microscopy[2] and then in reversible saturable optical fluorescence transitions (RESOLFT) imaging.[8]

In contrast to STED and GSD, RESOLFT implements reversibly photoswitchable fluorescent proteins (rsFPs) as imaging probes.[14−17] The photoswitching of rsFPs between high (ON) and low (OFF) fluorescent states permits a >100 000-fold decrease in switching the OFF intensity (in contrast to depletion in STED), compared to conventional STED/GSD techniques, employing constitutively fluorescent probes. Important characteristics that determine the successful use of rsFPs in RESOLFT include their photoswitching contrast, photoswitching half-times, and photoswitching fatigue resistance (Figure 1). The photoswitching contrast (defined as the ratio of fluorescence intensities, I^{ON}/I^{OFF}) determines the overall performance of an rsFP. Ideally, rsFPs should have switching kinetics suitable for both high-speed and low-intensity imaging, as the latter case requires longer exposures, thus increasing pixel dwell time. Finally, resistance to photoswitching fatigue permits execution of a large number of switching cycles, thus improving the signal-to-noise ratio of an image.

All currently available rsFPs belong to the green fluorescent protein (GFP)-like[16,17] family of proteins. They have been used in wide-field diffraction-limited intracellular photolabeling and tracking, as well as in super-resolution RESOLFT microscopy. However, their application to deep-tissue imaging are limited, because none of them have excitation and emission maxima in the near-infrared (NIR) tissue transparency window (~650−900 nm).[18]

Recently, several constitutively fluorescent NIR FPs, (i.e., iRFPs), were developed from bacterial phytochromes

Received: September 5, 2016
Accepted: November 3, 2016
Published: November 3, 2016

DOI: 10.1021/acs.analchem.6b03499
Anal. Chem. 2016, 88, 11821−11829

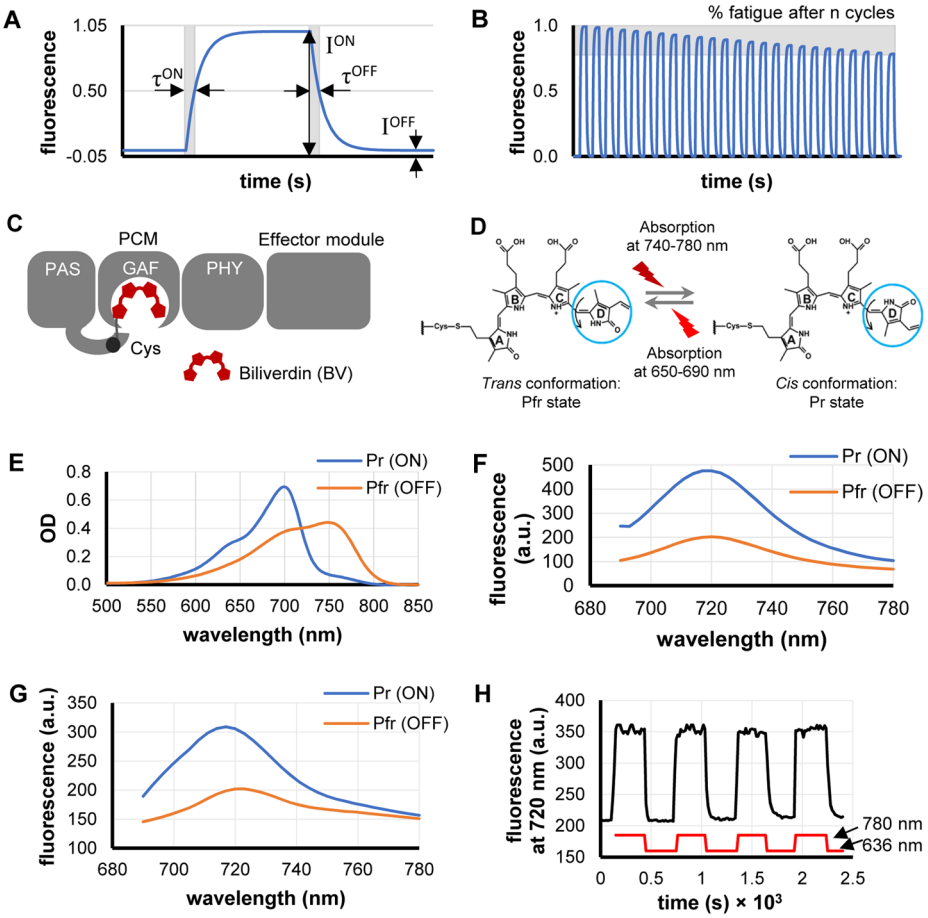

Figure 1. Characterization of DrBphP-PCM reversible photoswitching and major parameters that should be optimized. (A) Each rsFP photoswitching cycle is characterized by switching contrast, which is the ratio of fluorescence intensities (I^{ON}/I^{OFF}), as well as by half-times of photoswitching ON (τ^{ON}) and OFF (τ^{OFF}). (B) Photofatigue of an rsFP is denoted as the relative decrease of the I^{ON} fluorescence intensity after n cycles of reversible switching. (C) A monomer of the full-length DrBphP bacterial phytochrome consists of a PCM module (PAS, GAF, and PHY domains) and an effector module. (D) Biliverdin (BV) molecule bounded to DrBphP undergoes a cis−trans isomerization of the C15/C16 double bond in its D-ring (blue circle) during photoconversion. (E, F) Absorbance (panel (E)) and fluorescence (panel (F)) spectra of DrBphP-PCM protein solution in the Pr state (ON; blue line) and after photoconversion to the Pfr state (OFF; orange line). (G) Fluorescence spectra of the suspension of live HeLa S3 cells stably expressing DrBphP-PCM protein in the Pr state (ON; blue line) and after photoconversion to the Pfr state (OFF; orange line). (H) Repeated fluorescence changes of the suspension of HeLa S3 cells stably expressing DrBphP-PCM protein detected at 720 nm during recurrent illumination cycles with 780/20 nm (switching on) and 636/20 nm (switching off). Measurements in panels (E)−(H) were performed in cuvettes in a commercial spectrophotometer (panel (E)) and steady-state fluorometer (panels (F)−(H)).

(BphPs).[16,19] The BphP-derived family of iRFPs employs the mammalian-cell-abundant linear tetrapyrrole biliverdin (BV), as a chromophore. BphPs contain a photosensory core module (PCM), which is comprised by PAS, GAF, and PHY domains, and an output effector module (Figure 1C).[20,21] The BV chromophore is covalently bound to a cysteine residue at the N-terminus of the PAS domain and located within a pocket of the GAF domain. The PCM module is mainly responsible for the photophysical properties of BphPs, which can exist in two stable interconvertible spectral states: far-red absorbing (Pr) and NIR absorbing (Pfr), associated with cis and trans photoisomerization of BV, respectively (Figure 1D). The PCM is the minimal BphP fragment that can efficiently and reversibly photoconvert between Pr and Pfr states, but NIR rsFPs based on PCMs are not yet available, despite the high potential for this class of fluorophores. Engineering of the PCM of AtBphP2 from *Agrobacterium tumefaciens* to photoactivatable proteins, PAiRFPs, which photoconvert only once, represents a first step in this direction.[22] PAiRFPs have been selectively photoactivated within small regions of tissue in mice, but several drawbacks impede their further use in super-resolution imaging.[22]

To date, the properties of GFP-like rsFP have been optimized by multiple rounds of screening of large cell-based libraries. There are three major techniques available for high-throughput screening and sorting of cells: fluorescence-activated cell sorters (FACSs), robotic microtiter assay, and custom microfluidic-based systems. Manipulation of switching contrast and photostability requires complex approaches where excitation wavelength, irradiance, pulse sequence, and exposure times are tailored to properly extract the correct photophysical parameters.[23−25] For example, screening for photoswitching requires a dedicated set of excitation beams to realize at least one cycle of in-flow photoconversion, whereas screening for low fatigue requires additional beams and delay lines for tracking fluorescence changes under controllable photobleaching. Because of the relatively slow photoconversion kinetics of rsFPs and BphPs,[22,26,27] a time window from tens to hundreds of milliseconds is required to complete all measurements, which then must be analyzed for each cell in real time while it moves

DOI: 10.1021/acs.analchem.6b03499
Anal. Chem. 2016, 88, 11821−11829

in the flow path. These factors make it impossible to use a conventional FACS, because of its high speed and virtually nonconfigurable arrangement of excitation beams. Photoswitching of single MTLn3 carcinoma cells labeled with the rsFP Dendra2 has been observed with a custom-built optical setup both on glass slides and within blood vessels in mice.[28] Although this approach represents a key step in the evolution of the instrumentation with some of the necessary functionality for screening rsFP libraries, such as the appropriate multipulse excitation and timing, it does not enable selection of single cells. In contrast, microfluidics systems provide excellent flexibility: they allow for an arbitrary number of excitation beams, varying the time and order of excitation/read-out beams, long time delays,[29,30] and accurate cell sorting.[31]

Here, we describe a microfluidic in-flow multiple cycle photoswitching assay for NIR rsFPs. Diffractive optics are used to generate a two-color multiple-beam illumination pattern, which is matched to a fluidic channel geometry appropriate for the pulse sequence probing photoswitching. We used droplets of purified constitutively fluorescent iRFP713 as a calibration sample to compensate for beam-to-beam intensity variations.[32] To assess the effects of operating parameters on measurements of photoswitching in flow, we employed DrBphP-PCM, which is the BphP from *Deinococcus radiodurans*. This construct is a potential template for the development of new NIR rsFPs, because it has been successfully used to engineer constitutively fluorescent iRFPs.[18] To our knowledge, this is the first flow system that permits screening of NIR rsFPs on the basis of their most critical photophysical properties. The methods reported here represent a foundation for the design of high throughput screening systems enabling the development of rsFPs for super-resolution imaging, and other biophotonic functionalities for visualizing cellular phenomena.

EXPERIMENTAL SECTION

Protein Expression, Purification, and Characterization. DrBphP-PCM and iRFP713 with N-terminal polyhistidine tags were expressed and purified as described.[32] To determine fluorescence quantum yield of DrBphP-PCM, we compared fluorescence intensity of the purified protein to that of an equally absorbing iRFP713.[32] Photoconversion of purified protein solution (10 μM) or suspension of mammalian cells stably expressing DrBphP-PCM was measured with 5 mW/cm^2 of 780/20 nm and 636/20 nm LED sources.

Protein Expression in Mammalian Cells. We obtained a HeLa S3 (ATCC) stable preclonal mixture by transfecting cells with pDrBphP-PCM mammalian expression plasmid. Transfected HeLa S3 cells were selected for DrBphP-PCM expression with 700 μg/mL of G418 antibiotic and further enriched using a FACSAria sorter (BD Biosciences). The brightest cells expressing DrBphP-PCM were collected in the 710/20 nm fluorescence channel.

Single-Point Photoswitching Measurements. For single droplet measurements, purified protein samples were placed in a microwell 8 μm in diameter and 10 μm deep, closed with a coverslip. For single cell measurements, cell suspension was placed between two coverslips and sealed. The samples were illuminated with a pulse sequence consisting of a NIR (783 nm) pulse of 4 kW/cm^2, followed by three equally spaced red (643 nm) laser pulses of 1.2 kW/cm^2. This illumination corresponds to a single switching cycle, which starts by switching the protein on with the 783 nm laser and continues with stepwise switching off by the 643 nm laser. Each measurement consisted of 250 switching cycles.

Design of the Microfluidic Chip. Microfluidic chips were fabricated with polydimethylsiloxane (PDMS), using soft-lithography techniques. We used a flow-focusing junction for droplet generation as this geometry offers robust performance over a wide range of operating conditions.[33] Calculations of the chip geometry and its hydrodynamic properties used the model and algorithms described earlier.[34,35] The microfluidic chip has channels with 40 μm square cross-section, and both aqueous and oil phase channels are 50 mm long. The channels were treated with 1% perfluorododecyltrichlorosilane solution. This configuration produces ~2−3 50 pL droplets/s, moving with a speed that is adjustable in the range of 10−30 mm/s at input pressures of 1−2 psi. Driving pressure was applied to the microfluidic chip through $^1/_{16}$-in.-diameter PFA microtubings connected to precision dual-stage pressure regulators with an accuracy of 0.01 psi at the output stage. We used two separate regulators to adjust input pressures in aqueous- and oil-phase channels independently.

Design of the Optical System. In the optical setup (Figure 2), red and pink areas show traces of one (extreme) of

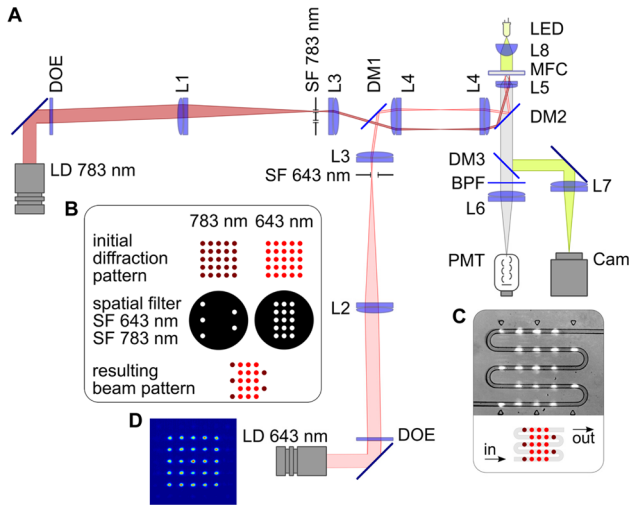

Figure 2. Experimental setup. (A) Optical scheme, where laser diode (LD) modules emitting at 643 and 783 nm, diffractive optical elements (DOEs), lenses L1−L5, dichroic mirrors DM1 and DM2, and custom-made spatial filters (SF 643 nm and SF 783 nm) comprise the illumination arms of the system. The detection part consists of a dichroic mirror (DM3), a bandpass filter (BPF), a lens (L6), and a photomultiplier tube (PMT). Lenses L5 and L7, and the light-emitting diode (LED), comprise the trans-illumination bright-field microscope used for targeting and monitoring. (B) Formation of the multiple-beam structured illumination pattern. (C) Schematic and microscopic image of interrogation region of the microfluidic chip with serpentine channel, where droplets interact with laser beams. (D) Intensity distribution in the initial 643 nm diffraction pattern.

the beams in the 643 and 783 nm illumination arms. The illumination optics generate 40-μm-diameter beams separated by a center-to-center distance of 130 μm, which was chosen to minimize beam overlap and provide dark relaxation times comparable to or longer than exposure times. This particular pattern gives dark relaxation times equal to twice the exposure time. The length of the beam waist (Rayleigh range) is ~1 mm, which greatly exceeds the 40 μm channel depth, thus ensuring that defocusing (axial displacement of the chip) minimally

DOI: 10.1021/acs.analchem.6b03499
Anal. Chem. 2016, 88, 11821−11829

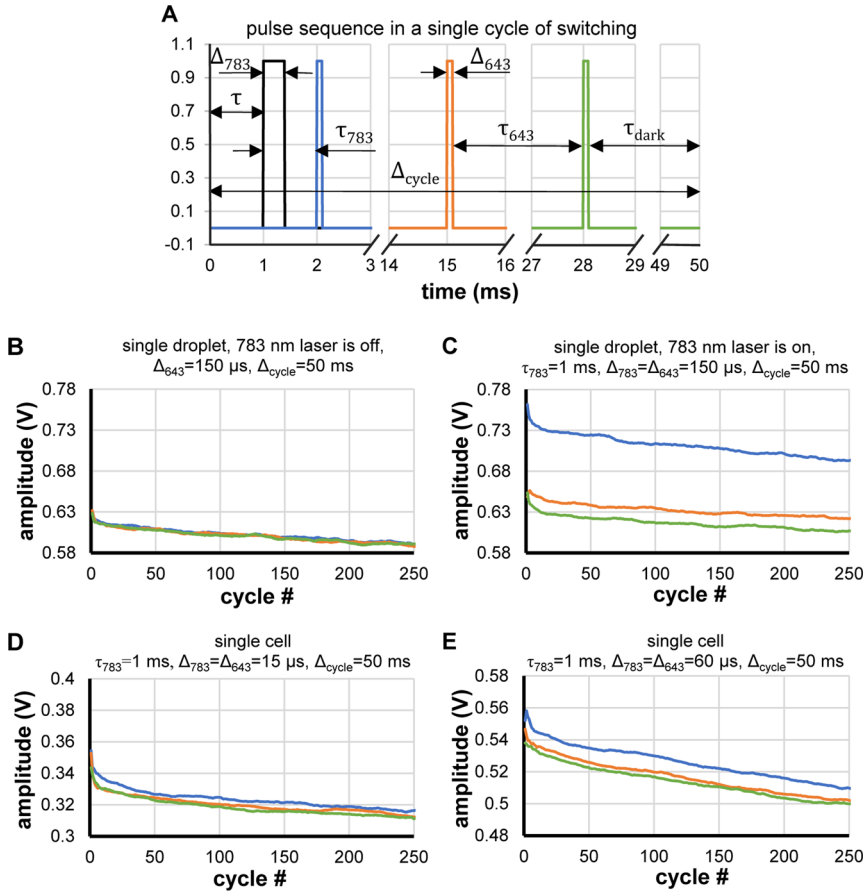

Figure 3. Single-point measurements of DrBphP-PCM photoswitching. (A) Pulse sequence used for photoswitching/excitation of a single droplet/single cell: τ_{643} = 13 ms, dark relaxation time τ_{dark} ($\tau_{dark} = \Delta_{cycle} - 3\Delta_{643} - 2\tau_{643} - \Delta_{783} - \tau$). (B, C) Measurements with a single droplet of 30 μM DrBphP-PCM solution: (B) 783 nm laser is off, photoswitching does not occur, slow decrease in amplitude indicates bleaching by 643 nm laser; and (C) 783 nm laser is on, different amplitudes of pulses show that stable photoswitching occurs within 250 cycles. (D, E) Measurements of the protein photoswitching in a single cell at different pulse durations/energies.

impacts the measured signal. All software required for acquisition and processing of optical signals was written in NI LabVIEW, using the NI DAQmx library to access the data acquisition board. Operational software allowed acquisition of the signal triggered by the first pulse in series, finding amplitude and position of pulses in the acquired signal, real-time calibration of amplitudes, and calculation of the switching contrast for every droplet.

RESULTS

Characterization of DrBphP-PCM Photoswitching in Ensemble. In the Pr (ON) state, purified DrBphP-PCM exhibited an absorbance maximum at 700 nm (Figure 1E), an emission maximum at 720 nm (Figure 1F), and a fluorescence quantum yield of 2.9%. Upon 636 nm illumination, it photoconverted to the Pfr (OFF) state with an absorbance maximum at 750 nm and a switching contrast of 230% for fluorescence intensity in the spectral range of 690−740 nm (Figure 1F). The absorbance at 700 nm also decreased almost 2-fold in the Pfr state. Similar fluorescence behavior was observed in HeLa S3 cells stably expressing DrBphP-PCM (Figure 1G). We next detected repetitive reversible photoswitching of DrBphP-PCM fluorescence in cell suspension. Under these conditions, DrBphP-PCM was photostable over several photoswitching cycles, with a switching contrast of 150% (Figure 1H).

Off-Chip Measurements of DrBphP-PCM Photoswitching. To determine microfluidic chip operating parameters such as flow speed (i.e., exposure and dark times) and excitation/switching laser energies, we measured photoswitching on stationary single droplets of purified DrBphP-PCM and single HeLa S3 cells expressing DrBphP-PCM under similar conditions. Microsecond laser pulses were used to simulate the passage of droplets through CW beams in a microchannel. The pulse sequence and duration for one illumination cycle are shown in Figure 3A, where the black curve represents a 783 nm laser pulse, and blue, orange, and green lines are successive 643 nm laser pulses. Although the 643 nm pulses are all of equal intensity, this sequence can be thought of as "on-probe−off-probe." The fluorescence response of the sample was quantified from the amplitudes of the signal pulses. The data shown in Figures 3B−E, as well as Figures S2−S4 in the Supporting Information were processed with a 30−50-point moving average filter. Photoswitching is evident from changes in signal amplitudes from the 643 nm pulses within a cycle. When the 783 nm laser is off, responses from the 643 nm excitation pulses within a cycle are equal (Figures 3B and S2C). However, when the 783 nm pulse is on, the fluorescence signal from the first 643 nm pulses is substantially higher, but the signal then decreases for the next two pulses, because the 643 nm pulses switch off the fluorescence. Figures 3B−E show dependence of signal pulse amplitude on the number of cycles, where line

DOI: 10.1021/acs.analchem.6b03499
Anal. Chem. 2016, 88, 11821−11829

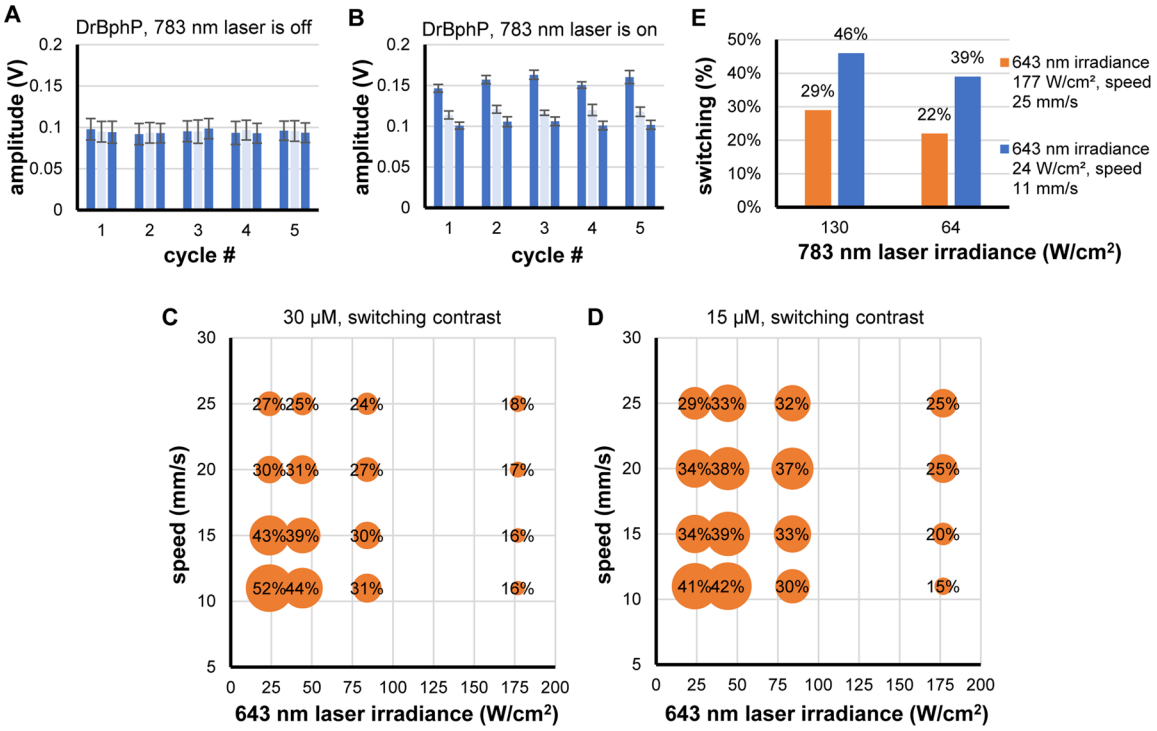

Figure 4. In-flow photoswitching of DrBphP-PCM protein: (A) amplitudes of fluorescent pulses from DrBphP-PCM droplets when 783 nm laser is off and photoswitching does not occur; (B) amplitudes of fluorescent pulses from DrBphP-PCM droplets when the 783 nm laser is on and photoswitching occurs; (C, D) dependence of switching contrast on intensity of the 643 nm laser and speed of droplets for 30 μM and 15 μM DrBphP-PCM protein solutions; and (E) dependence of photoswitching contrast on intensity of the 783 nm laser for 15 μM DrBphP-PCM protein solution.

color corresponds to the pulse colors in Figure 3A. The decrease of pulse amplitude with increasing number of cycles is caused by photobleaching. We varied the time delay between 783 nm pulse and 643 nm pulses (τ_{783}), length of the switching cycle (Δ_{cycle}), and pulse duration (Δ_{643} and Δ_{783}). In droplets of purified DrBphP-PCM, we discovered that the magnitude of photoswitching (vertical shift between blue and green points in the plots) is dependent on the time delay (τ_{783}). The highest switching response (illustrated in Figure 3C) was observed for τ_{783} = 1 ms. Longer τ_{783} caused a decrease in switching response (Figures S3A–C in the Supporting Information). This effect is caused by photoswitching upon exposure to low-intensity ambient light, because of the high light sensitivity of DrBphP-PCM. To reduce the influence of this ambient light as much as possible, all measurements were made in the dark room with sample that had been additionally covered from the back side. Further light insulation did not cause considerable improvements in switching response.

Next, we varied the dark time of a single switching cycle, i.e. cycle length Δ_{cycle} (Figure 3A). This parameter influences the transition of the protein into the ON (Pr) state due to exposure to ambient light between consecutive pulse cycles. This effect is easily revealed when the 783 nm laser is off. In this case, all three fluorescence pulses within a cycle should ideally have equal amplitudes, as seen in Figure 3B, where Δ_{cycle} = 50 ms. However, Figures S3D–F show that a small but measurable amount of switching occurs at Δ_{cycle} = 100 ms and Δ_{cycle} = 200 ms. Therefore, single-cell measurements were made using τ_{783} = 1 ms to ensure highest switching response and Δ_{cycle} = 50 ms to reduce the impact of uncontrollable transition of DrBphP-PCM into the Pr state.

In single-cell experiments, we varied the total energy exposure by varying pulse durations Δ_{643} and Δ_{783} from 15 μs to 100 μs, with fixed irradiances at 643 and 783 nm. These exposures correspond to fluences of 0.018–0.119 J/cm^2 at 643 nm and 0.060–0.398 J/cm^2 at 783 nm. Photoswitching was observed, even at the lowest exposures (Figure 3D). The highest switching response and largest amplitude signal were achieved at Δ_{643} = Δ_{783} = 60 μs (Figure 3E). Longer pulses did not significantly enhance either the switching response or signal amplitude (see Figures S4A–D in the Supporting Information). Based on this observation, we therefore determine the optimal conditions to observe in-flow switching of DrBphP-PCM in the microfluidic chip are 0.240 J/cm^2 at 783 nm and 0.072 J/cm^2 at 643 nm. Assuming a beam diameter of 40 μm and droplet speed of 10 mm/s, we obtain an exposure time of 4 ms and irradiances required in the microfluidic chip are 60 W/cm^2 CW at 783 nm, and 18 W/cm^2 CW at 643 nm. Using these intensities ensures identical switching conditions in both stationary off-chip experiments and in-flow measurements in the microfluidic chip.

Optical and Microfluidic System Design. The use of identical DOEs vastly simplifies management of the number and order of beams in the final diffraction pattern, thus allowing customization of the pulse sequence in the cytometry system, although at the cost of laser power approximately proportional to the number of beams that are blocked. Thus, for example, we used 15 of 25 643 nm beams and 5 of 25 783 nm beams in the initial diffraction pattern. Figures 2D and 2E show intensity distributions for the 643 nm laser beams measured in the object plane, where the microfluidic channels were placed (783 nm laser is turned off and spatial filter SF 643 nm is removed). The variation in beam intensity over the entire pattern is 10%,

DOI: 10.1021/acs.analchem.6b03499
Anal. Chem. 2016, 88, 11821–11829

excluding the zero-order beam, which has an intensity that is 30% higher than the mean value. To account for the effect of these variations on flow measurements, we performed calibrations with constitutively fluorescent iRFP713 (see below). As shown below, the 783 nm beam intensity only weakly impacts the switching contrast, and therefore, we neglected calibration for the 783 nm laser beams.

We folded the fluidic channel multiple times into a geometry that matches the two-dimensional array of beams from the DOE (Figure 2C) and provides a sufficient length within the field of view of the imaging system. Generally, the number of cycles chosen is a compromise between complexity of the signal to be analyzed and consistency of the analysis. Our current design permits up to five cycles of switching, and any cycle can be excluded from analysis individually using a spatial filter.

Chip design requires optimization of the channel geometry using a set of initial parameters, such as the viscosity and density of the liquids, a usable range of driving pressures, and a set of desired properties of the droplets, such as volume, speed, and spacing. Droplet frequency and speed are the most important operating parameters, because they must take into account the photoswitching kinetics of DrBphP-PCM.[22,26,27] Given the intensities and diameters of the laser beams and distances between them, low speeds ensure sufficient exposure times for droplets to absorb sufficient energy for photoswitching and for conformational changes in the protein to occur. At the same time, the speed and frequency of the droplets should be high enough for the system throughput to be at a reasonable level. The compromise between these factors resulted in the droplet generator used in our study, which gave a droplet volume of ∼50 pL, a droplet frequency of 2−3 droplets/s, and a speed of 10−30 mm/s at 1−2 psi driving pressure.

Constitutively Fluorescent NIR FP. To compensate for fluctuations in the fluorescence signal due to a nonuniform distribution of the 643 nm beam intensities in the diffraction pattern, we performed calibrations with droplets of purified constitutively fluorescent iRFP713, which has an excitation peak at 690 nm and emission maximum at 713 nm.[32] Figure S5A in the Supporting Information shows typical signals from a droplet of iRFP713 in flow. To ensure that photobleaching of iRFP713 does not affect the accuracy of the calibration, we performed time-lapse measurements with a single beam exciting a single motionless droplet filled with iRFP713. Figures S6A and S6B in the Supporting Information show that bleaching does not exceed 1% within the first 200 ms. In flow, droplets move at a speed of 10−30 mm/s and pass through a 40-μm-diameter laser beam in 2−4 ms. The time needed for a droplet to pass the entire interaction region is ∼200 ms (Figure S5A). Assuming that all pulses from a single droplet should be of equal amplitude, one can calculate an array of calibration coefficients (i.e., a lookup table, LUT).

Reversibly Switchable NIR FP Variant. We studied DrBphP-PCM in flow under various conditions, such as droplet speed and continuous wave intensities of 643 and 783 nm lasers (Table S1 in the Supporting Information). Figures 4A and 4B illustrate the fluorescence responses of DrBphP-PCM in flow. The switching contrast was calculated as a ratio of amplitudes of the first-pulse responses to third-pulse responses within a cycle (blue bars in the plot). This ratio was calculated for every cycle of switching and averaged over all cycles. Amplitude of the second pulse (light blue bar) served as an additional parameter sensitive to the kinetics of switching. Bar plots in Figures 4A and 4B show amplitudes averaged over 200 droplets. To verify that photoswitching occurs, we examined a signal from DrBphP-PCM when 783 nm laser is off. Figure 4A shows that amplitudes of the pulses are equal within 6% error. In contrast, when the 783 nm laser is on (Figure 4B), switching is clearly visible in every cycle.

We found that the 643 nm excitation (switching-off) laser irradiance has a considerable and complex effect on the switching contrast. It was expected that, with decreasing droplet speeds, the switching contrast should increase, as longer exposure ensures complete photoswitching. However, near the maximum values of 643 nm irradiance examined here (178 W/cm^2), we find an inverse relationship. With decreasing irradiance, the influence of exposure time is weak (near 84 W/cm^2) and then directly proportional to irradiance in the range of 20−45 W/cm^2. Even though PDMS is transparent at these wavelengths, laser light scatters from impurities and reflects from interfaces within the chip, leading to switching between excitation pulses. At low droplet speeds, the impact of this incidental switching increases and, at an extreme irradiance of 178 W/cm^2, results in a greatly decreased photoswitching contrast.

We observed a difference in the photoswitching response of 15 μM and 30 μM droplets of DrBphP-PCM. The most significant differences are seen at the minimal and maximal values of 643 nm irradiance, revealing an inverse relationship between switching contrast and droplet speed. This behavior can be understood by considering that lower concentrations of DrBphP-PCM requires less energy to be switched in both directions, while higher concentrations of droplets demonstrate substantial inertia in photoswitching.

The influence of the NIR laser irradiance on switching was much weaker (Figure 4E). At half of the maximum 783 nm laser irradiance, a relatively high 40% switching contrast was observed, whereas 45% was achieved with maximum irradiance, while adjustment of the droplet speed and irradiance of 643 nm laser beams produced changes of the switching contrast in the range of 15%−50%. Most likely, the 783 nm laser did not promote considerable switching between beams, because of the lower scattering of long-wavelength irradiation, at least within the available laser power.

Dotplots of switching contrast versus brightness were made for droplets of 1.8, 7.5, 15, and 30 μM DrBphP-PCM in flow. For example, Figure 5A shows a dotplot for 10 000 droplets of 15 μM DrBphP-PCM measured both with the 783 nm laser off and on, and averaged over all five cycles. Dotplots for droplets filled with 1.8, 7.5, and 30 μM DrBphP-PCM are shown in Figure S7 in the Supporting Information. Values to the left and below each cluster give the coefficients of variation (CV) of the switching contrast and brightness, respectively. The cluster of points near the bottom left is collected with the 783 nm switching laser off (highlighted green area), whereas the other pair, near 20%−40%, are measured with the laser on (highlighted red area).

For the points collected with the 783 nm laser on, the cluster at the highest contrast value represents switching contrast versus brightness for the droplet from the first 643 nm beam and the other represents measurements from the second 643 nm beam. In both cases, the signal (brightness) from the third pulse is used to calculate the contrast ratio, i.e.,

$$\text{contrast ratio} = \frac{\langle \text{brightness in the first pulse} \rangle}{\langle \text{brightness in the third pulse} \rangle} \qquad \text{for beam 1}$$

DOI: 10.1021/acs.analchem.6b03499
Anal. Chem. 2016, 88, 11821−11829

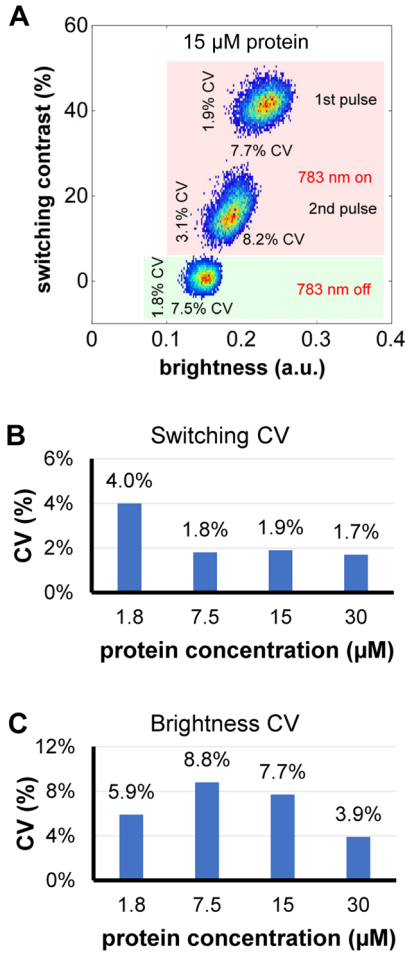

Figure 5. Dependence of switching contrast on brightness of droplets with DrBphP-PCM protein: (A) dotplot and coefficients of variation (CVs) for the 15 μM protein solution; (B) dependence of the CV of switching contrast on protein concentration; and (C) dependence of CV of brightness on protein concentration.

and

$$\text{contrast ratio} = \frac{\langle \text{brightness in the second pulse} \rangle}{\langle \text{brightness in the third pulse} \rangle} \qquad \text{for beam 2}$$

The rationale for this choice is that, after the second 643 nm switching-off beam, it is assumed that the entire population is now in the OFF (Pfr) state. This can be seen in that the shift between clusters of points along the horizontal axis is larger, because the droplets are initially turned on by the 783 nm beam in each cycle and, therefore, the first 643 nm beams have the largest effect on switching the fluorescence off. Figures 5B and 5C, as well as Figure S7 in the Supporting Information, show the dependence of the CVs on concentration of the protein solution for the first pulse (highest switching contrast and highest brightness). Interestingly, even though dispersion of the brightness is relatively high (and we can assume that it is not dependent on concentration), because of the droplet-to-droplet variation of the brightness, the CV of the switching contrast values is very small. Changes in brightness are obviously caused by changes in droplet size and speed; however, these changes do not influence the performance of the system and, therefore, the switching contrast can be calculated with very high precision. Even for the lowest concentration of 1.8 μM, the CV of the switching coefficient is only 4%, which means deviation of the switching coefficient is an order of magnitude lower than its mean value. Droplet-to-droplet variation of the brightness caused by changes in droplet size can be reduced further by introducing droplet size sensor based on either detection of scattered light or microscopic image recognition. Although other representations of these rather high-dimensional data can be considered, we expect the dotplots shown to be of significant value in quantifying the photoswitching performance of rsFPs (for example, in the screening of libraries).

DISCUSSION

The innovative features of our microfluidic system arise from a combination of two factors: (i) simplicity of the system (i.e., simple design of the microfluidic chip, diffractive-optics-based multiple beam illumination, rigid optical scheme) and (ii) complex analysis possible with this simple scheme (i.e., multiple cycles of switching, multiple variations in the beam arrangement). Applications of microfluidics to single cell, particularly fluorescence-activated, analysis have expanded considerably through the past decade. An important category of these applications concerns systems that reside in two distinct states. These states may, for example, correspond to ligand bound/unbound states of a sensor for some cellular analyte, or activated/deactivated states of an optogenetic element controlling a signaling pathway. Although many reports describe cell manipulation within single-cell traps and cell arrays[36,37] few publications describe multiple in-flow operations on single droplets or cells[23−25,38] as would be necessary for profiling and sorting populations.

For example, Dolega et al.[39] have proposed the most direct implementation of such a system using multiple valves for iterative routing of a droplet through a chip. Using multiple valves requires precise and complex synchronization, especially at higher speeds of operation. Their system incorporates long droplet residence times in a looped microfluidic channel to study crystallization and precipitation processes in droplets. Screening for photoswitching efficiency in such a system would be impractical, because of the long residence times, relative to the photoswitching kinetics of rsFPs. Another report describes an interesting idea,[40] where environmental conditions within the microfluidic chip were reversibly changed by varying solution flow rates, similar to the sheath flow in the flow-focusing junction, and optical tweezers were used for precise positioning of a cell in the flow. Although this scheme allows iterative single-cell analysis, realization of a high-throughput screening system on this basis is unrealistic. Therefore, the work reported here represents a substantial advance, because it is the first to describe in-flow triggering, probing, and quantification of multiple reversible photoswitching of DrBphP-PCM both in single-point and in-flow experiments.

For measurements of switching contrast in a cell population, accuracy of estimation and the influence of exogenous factors are crucial. One of these factors is spontaneous or uncontrollable switching, which can be systematic and cause bias of estimation. For example, single-point measurements showed that switching contrast was dependent on time delay between illumination of the sample with the 783 nm laser (switching protein ON) and illumination with the 643 nm laser (excitation/switching protein OFF). Switching contrast decreased as the time delay increased (see Figures S3A−C). This effect is due to the uncontrollable transition of the DrBphP-PCM protein into the Pfr state under the influence of weak

DOI: 10.1021/acs.analchem.6b03499
Anal. Chem. 2016, 88, 11821−11829

ambient light. Excessive time delay between consecutive switching cycles caused early transition of the protein into the ground Pr state (Figure S3D−F). Competitive influence of these two opposite processes in the microfluidic chip overlapped with other factors, such as protein concentration. In agreement with measurements on stationary droplets, we found that the low droplet speed/low intensity of the 643 nm laser provide optimal conditions for observing high photoswitching contrast in flow (Figure 4). However, single-point experiments showed that, although it is possible to use higher excitation intensity at 643 nm (Figure 3), switching contrast does not increase, although the magnitude of the signal does increase. This flexibility will facilitate switching measurements on rsFPs in cells over a range of dimensions and expression levels. Note that the rather low (2.9%) fluorescence quantum yield of DrBphP-PCM represents the lower bound of what will be of interest in efforts to develop new rsFPs.

Both types of measurement described here, single-point and in-flow, demonstrate the ability of DrBphP-PCM to be reversibly and repeatedly photoswitched and used as a calibration standard for in-flow measurements. Moreover, single-point measurements provided clear evidence that the protein withstands at least 250 cycles of consecutive switching without a substantial reduction in photoswitching contrast. During photoswitching, DrBphP-PCM undergoes structural rearrangements. Upon illumination with far-red light, the C15═C16 double bond in the biliverdin isomerizes from cis to trans conformation. It leads to a concomitant reorientation of the hydrogen bond network around D-ring and adjacent amino acids residues of the protein. These combined motions are followed by complex structural remodeling of the PAS-GAF-PHY triad domains.[41] The observed decrease in photoswitching contrast after the increase in delay time between illumination with red and NIR lasers could be explained by the fast reverse BV isomerization caused by exposure to ambient light.

The developed system operates on principles similar to those of conventional flow cytometers but provides multidimensional data with substantially more information content. Because of the combination of the robust optical system, a simple, flexible, and cost-effective droplet-based microfluidics technique, and a specialized calibration procedure for both intensity and switching our system proposes screening based on the unique property of the rsFPs, such as the efficiency of switching. Measurement of the switching contrast has been achieved with a hardware-limited CV of the system of as low as 1.7%, because droplet-to-droplet fluctuations in the fluorescent signal are suppressed by the ratiometric quantity. Since this system operates under steady-state flow conditions, we expect that actuation methods such as dielectrophoresis can easily be implemented to subsequently sort the droplets with criteria based on the brightness, photoswitching contrast, switching fatigue, or any changes in spectral properties (e.g., absorbance) of the cells/proteins/particles contained within them.

CONCLUSION

We developed the first system for in-flow switching and screening of near-infrared (NIR) reversibly photoswitchable fluorescent proteins (rsFPs), which consits of diffractive optics for a multiple-beam illumination pattern and droplet-based microfluidics to interrogate cell-sized volumes of the protein. This system enabled observation of several consecutive cycles of reversible photoswitching of the weakly fluorescent protein bacterial phytochrome photosensory core module from *Deinococcus radiodurans* (DrBphP-PCM) in droplets flowing through a microfluidic channel. We determined the optimal conditions necessary to observe the highest contrast of in-flow switching. Finally, we tested the system in flow-cytometry mode with droplets filled with purified protein solution to characterize and to visualize population of droplets in industry-accepted form. The real-time analysis capability of this system makes it straightforward to incorporate cell-sorting functionality, thereby providing a solid basis for microfluidics-based directed evolution of NIR rsFPs.

ASSOCIATED CONTENT

Supporting Information

The Supporting Information is available free of charge on the ACS Publications website at DOI: 10.1021/acs.analchem.6b03499.

Details on optical system, formation of structured illumination pattern, calibration procedure and additional data on single-point and in-flow switching experiments (PDF)

AUTHOR INFORMATION

Corresponding Authors

*Fax: 1 (303) 492-5235. E-mail: rjimenez@jila.colorado.edu (R. Jimenez).

*Fax: 1 (718) 430-8996. E-mail: vladislav.verkhusha@einstein.yu.edu (V. Verkhusha).

Notes

The authors declare no competing financial interest.

ACKNOWLEDGMENTS

We thank Janne Ihalainen (University of Jyväskylä, Finland) for the DrBphP gene, Clark Lagarias (University of California at Davis) and Richard Vierstra (University of Wisconsin at Madison) for the plasmids for production of biliverdin in bacteria, and Brett Fiedler (JILA, University of Colorado at Boulder) for helpful discussions. This work was supported by the GM108579 and GM105997 grants from the U.S. National Institutes of Health (NIH) and by Grant No. ERC-2013-ADG-340233 from the EU FP7 program (to V.V.V.). R.J. is a staff member in the Quantum Physics Division of the National Institute of Standards and Technology (NIST). Certain commercial equipment, instruments, or materials are identified in this paper in order to specify the experimental procedure adequately. Such identification is not intended to imply recommendation or endorsement by the NIST, nor is it intended to imply that the materials or equipment identified are necessarily the best available for the purpose.

REFERENCES

(1) Hell, S. W.; Wichmann, J. *Opt. Lett.* **1994**, *19*, 780−782.
(2) Hell, S. W.; Kroug, M. *Appl. Phys. B: Lasers Opt.* **1995**, *60*, 495−497.
(3) Hell, S. W.; Schrader, M.; van der Voort, H. T. *J. Microsc.* **1997**, *187*, 1−7.
(4) Gustafsson, M. G. *J. Microsc.* **2000**, *198*, 82−87.
(5) Nienhaus, K.; Nienhaus, G. U. *J. Mol. Biol.* **2016**, *428*, 308−322.
(6) Cox, S. *Dev. Biol.* **2015**, *401*, 175−181.
(7) Shcherbakova, D. M.; Sengupta, P.; Lippincott-Schwartz, J.; Verkhusha, V. V. *Annu. Rev. Biophys.* **2014**, *43*, 303−329.
(8) Hell, S. W.; Jakobs, S.; Kastrup, L. *Appl. Phys. A: Mater. Sci. Process.* **2003**, *77*, 859−860.

DOI: 10.1021/acs.analchem.6b03499
Anal. Chem. 2016, 88, 11821−11829

(9) Betzig, E.; Patterson, G. H.; Sougrat, R.; Lindwasser, O. W.; Olenych, S.; Bonifacino, J. S.; Davidson, M. W.; Lippincott-Schwartz, J.; Hess, H. F. *Science* **2006**, *313*, 1642−1645.
(10) Rust, M. J.; Bates, M.; Zhuang, X. *Nat. Methods* **2006**, *3*, 793−795.
(11) Dempsey, G. T.; Vaughan, J. C.; Chen, K. H.; Bates, M.; Zhuang, X. *Nat. Methods* **2011**, *8*, 1027−1036.
(12) Dean, K. M.; Palmer, A. E. *Nat. Chem. Biol.* **2014**, *10*, 512−523.
(13) Shaner, N. C. *Methods Cell Biol.* **2014**, *123*, 95−111.
(14) Hofmann, M.; Eggeling, C.; Jakobs, S.; Hell, S. W. *Proc. Natl. Acad. Sci. U. S. A.* **2005**, *102*, 17565−17569.
(15) Grotjohann, T.; Testa, I.; Reuss, M.; Brakemann, T.; Eggeling, C.; Hell, S. W.; Jakobs, S. *eLife* **2012**, *1*, e00248.
(16) Shcherbakova, D. M.; Verkhusha, V. V. *Curr. Opin. Chem. Biol.* **2014**, *20*, 60−68.
(17) Subach, F. V.; Zhang, L.; Gadella, T. W.; Gurskaya, N. G.; Lukyanov, K. A.; Verkhusha, V. V. *Chem. Biol.* **2010**, *17*, 745−755.
(18) Shcherbakova, D. M.; Baloban, M.; Verkhusha, V. V. *Curr. Opin. Chem. Biol.* **2015**, *27*, 52−63.
(19) Shcherbakova, D. M.; Verkhusha, V. V. *Nat. Methods* **2013**, *10*, 751−754.
(20) Piatkevich, K. D.; Subach, F. V.; Verkhusha, V. V. *Chem. Soc. Rev.* **2013**, *42*, 3441−3452.
(21) Shcherbakova, D. M.; Shemetov, A. A.; Kaberniuk, A. A.; Verkhusha, V. V. *Annu. Rev. Biochem.* **2015**, *84*, 519−550.
(22) Piatkevich, K. D.; Subach, F. V.; Verkhusha, V. V. *Nat. Commun.* **2013**, *4*, 2153.
(23) Dean, K. M.; Davis, L. M.; Lubbeck, J. L.; Manna, P.; Friis, P.; Palmer, A. E.; Jimenez, R. *Anal. Chem.* **2015**, *87*, 5026−5030.
(24) Davis, L. M.; Lubbeck, J. L.; Dean, K. M.; Palmer, A. E.; Jimenez, R. *Lab Chip* **2013**, *13*, 2320−2327.
(25) Lubbeck, J. L.; Dean, K. M.; Ma, H.; Palmer, A. E.; Jimenez, R. *Anal. Chem.* **2012**, *84*, 3929−3937.
(26) Bjorling, A.; Berntsson, O.; Takala, H.; Gallagher, K. D.; Patel, H.; Gustavsson, E.; St. Peter, R.; Duong, P.; Nugent, A.; Zhang, F.; Berntsen, P.; Appio, R.; Rajkovic, I.; Lehtivuori, H.; Panman, M. R.; Hoernke, M.; Niebling, S.; Harimoorthy, R.; Lamparter, T.; Stojkovic, E. A.; Ihalainen, J. A.; Westenhoff, S. *J. Phys. Chem. Lett.* **2015**, *6*, 3379−3383.
(27) Zienicke, B.; Molina, I.; Glenz, R.; Singer, P.; Ehmer, D.; Escobar, F. V.; Hildebrandt, P.; Diller, R.; Lamparter, T. *J. Biol. Chem.* **2013**, *288*, 31738−31751.
(28) Nedosekin, D. A.; Verkhusha, V. V.; Melerzanov, A. V.; Zharov, V. P.; Galanzha, E. I. *Chem. Biol.* **2014**, *21*, 792−801.
(29) Zagnoni, M.; Cooper, J. M. *Methods Cell Biol.* **2011**, *102*, 23−48.
(30) Ma, H.; Gibson, E. A.; Dittmer, P. J.; Jimenez, R.; Palmer, A. E. *J. Am. Chem. Soc.* **2012**, *134*, 2488−2491.
(31) Mazutis, L.; Gilbert, J.; Ung, W. L.; Weitz, D. A.; Griffiths, A. D.; Heyman, J. A. *Nat. Protoc.* **2013**, *8*, 870−891.
(32) Filonov, G. S.; Piatkevich, K. D.; Ting, L. M.; Zhang, J.; Kim, K.; Verkhusha, V. V. *Nat. Biotechnol.* **2011**, *29*, 757−761.
(33) Abate, A. R.; Poitzsch, A.; Hwang, Y.; Lee, J.; Czerwinska, J.; Weitz, D. A. *Phys. Rev. E Stat. Nonlin. Soft Matter Phys.* **2009**, *80*, 026310.
(34) Berthier, J.; Silberzan, P. *Microfluidics for Biotechnology*; Artech House: Boston, MA, 2010.
(35) Bruus, H. *Theoretical Microfluidics*; Oxford University Press: Oxford, U.K., 2007.
(36) Fu, A. Y.; Chou, H. P.; Spence, C.; Arnold, F. H.; Quake, S. R. *Anal. Chem.* **2002**, *74*, 2451−2457.
(37) Hong, J. W.; Studer, V.; Hang, G.; Anderson, W. F.; Quake, S. R. *Nat. Biotechnol.* **2004**, *22*, 435−439.
(38) Dean, K. M.; Lubbeck, J. L.; Davis, L. M.; Regmi, C. K.; Chapagain, P. P.; Gerstman, B. S.; Jimenez, R.; Palmer, A. E. *Integr. Biol.* **2015**, *7*, 263−273.
(39) Dolega, M. E.; Jakiela, S.; Razew, M.; Rakszewska, A.; Cybulski, O.; Garstecki, P. *Lab Chip* **2012**, *12*, 4022−4025.
(40) Eriksson, E.; Sott, K.; Lundqvist, F.; Sveningsson, M.; Scrimgeour, J.; Hanstorp, D.; Goksor, M.; Graneli, A. *Lab Chip* **2010**, *10*, 617−625.
(41) Takala, H.; Bjorling, A.; Berntsson, O.; Lehtivuori, H.; Niebling, S.; Hoernke, M.; Kosheleva, I.; Henning, R.; Menzel, A.; Ihalainen, J. A.; Westenhoff, S. *Nature* **2014**, *509*, 245−248.

DOI: 10.1021/acs.analchem.6b03499
Anal. Chem. 2016, 88, 11821−11829

Supporting Information

Microfluidic system for in-flow reversible photoswitching of near-infrared fluorescent proteins

Vladislav V. Lychagov[1,2], Anton A. Shemetov[1,2], Ralph Jimenez[3,4,*] and Vladislav V. Verkhusha[1,2,5,*]

[1]Department of Anatomy and Structural Biology and [2]Gruss-Lipper Biophotonics Center, Albert Einstein College of Medicine, Bronx, New York 10461, USA

[3]JILA, National Institute of Standards and Technology and [4]Department of Chemistry and Biochemistry, University of Colorado, Boulder, Colorado 80309, USA

[5]Department of Biochemistry and Developmental Biology, Faculty of Medicine, University of Helsinki, Helsinki 00029, Finland

Abstract

Here we present additional information on optical scheme functioning, formation of multiple beam structured illumination pattern, energy of excitation/switching irradiation used in experiments and principal scheme of the experimental setup. Next, we describe some additional results for single-point experiment, calibration procedure and in-flow switching experiment.

Details on experimental system

Design of optical system.

We used laser diode (LD) modules from Power Technology IQu2A100 and IQu2A105 emitting at 643 nm and 783 nm, respectively. To produce evenly spaced multiple beams of equal intensities, two identical diffractive optical elements (DOEs; HOLOEYE) were used (Figure 2A). Each element split the incident laser beam into 5×5 beams pattern with 0.1° at 640 nm (0.12° at 780 nm) angular distance between beams, along with suppression of higher orders of diffraction. Lenses L1, f_1=125 mm and L2, f_2=150 mm were used to handle these beams and to make the first intermediate diffraction patterns in the joint focal planes of lenses L1-L3 and L2-L3 (f_3=20 mm), where the spatial filters SF 783 nm and SF 643 nm were installed (Figure 2B). These filters were necessary to remove unwanted beams from the first intermediate diffraction patterns and to form the second, total intermediate diffraction pattern in the joint focal plane of lenses L4, f_4=50 mm. Dichroic mirror DM1 (Chroma T6851pxr) and lenses L4 were used to combine intermediate diffraction patterns from the 643 nm and the 783 nm lasers and to pass them with the help of the objective lens L5, f_5=10 mm into the object plane inside the microfluidic channels MFC. Additional beam stopper could be installed between lenses L4 to selectively remove any of five cycles of switching in the final beams pattern. Dichroic mirror DM2 (Chroma T660lpxr) reflects laser light toward the microfluidic chip MFC and transmits collected fluorescent signal toward the PMT (Hamamatsu R10699), and a light-emitting diode (LED) light toward the image sensor Cam. Dichroic mirror DM3 (Chroma 89016bs) separates fluorescence from LED light.

Electronics and detection.

Fluorescence photons collected by the optical system is detected by a PMT operated at – 600-700 V. Current output of the PMT loads input of a custom-built transimpedance amplifier with a gain of 300 V/A, and output voltage of the amplifier is digitized by the data acquisition (DAQ) board NI PCIe-6351. This DAQ board has analog outputs used for controlling laser diodes. Data acquisition and processing software along with utilities for controlling peripheral devices connected to PC were realized in the NI LabVIEW programming environment (Figure S1).

Table S1. Energy in J/cm^2, which a droplet receives in a single beam.

Wavelength, nm		643 nm				783 nm	
Exposure time, ms	Irradiance, W/cm^2 / Flow speed, mm/s	176.84	84.00	44.21	23.87	129.98	63.66
3.64	11	0.64	0.31	0.16	0.09	0.47	0.23
2.67	15	0.47	0.22	0.12	0.06	0.35	0.17
1.60	25	0.28	0.13	0.07	0.04	0.21	0.10

The intensity row contains values of average intensity in a single beam and the speed column specifies droplet speeds for which stable droplet generation and flow was possible. Exposure time was estimated from the beam diameter and droplet speed, and exposure energy was calculated as a product of fluence and exposure time.

643 nm laser diode intensity – 80 mW. 643 nm intensity on the sample with DOE installed, 25 beams – 55.5 mW. 643 nm intensity on the sample with DOE installed, 1 beam – 2.22 mW. 783 nm laser diode intensity – 90 mW. 783 nm intensity on the sample with DOE installed, 25 beams – 41 mW. 783 nm intensity on the sample with DOE installed, 1 beam – 1.63 mW. All measurements were made by Coherent LabMax-TO with VIS head.

Figure S1. Principal scheme of the experimental setup and the interconnections between the key components.

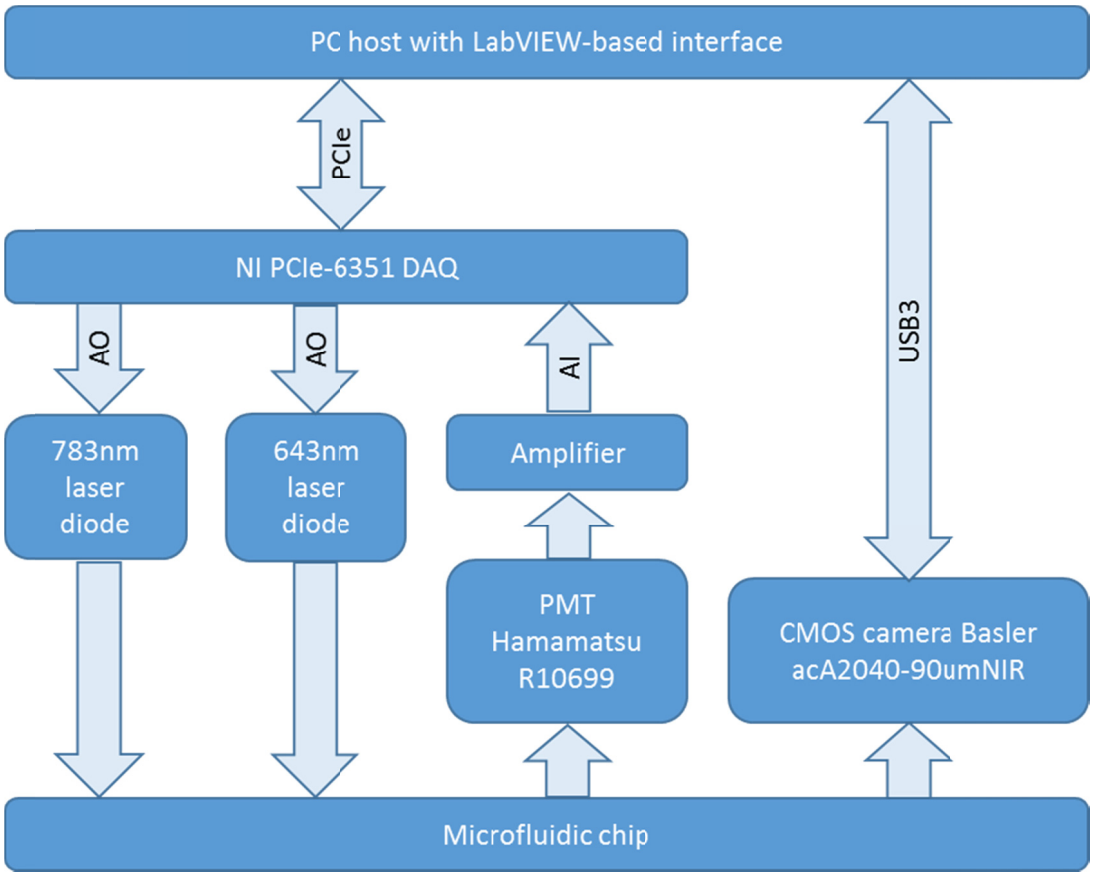

Figure S2. Examples of the raw pulsed signals (single photoswitching cycle) and changes in the signal amplitude with the number of photoswitching cycle. 783 nm pulse irradiance was 4 kW/cm^2 and 643 nm laser pulses were 1.2 kW/cm^2.

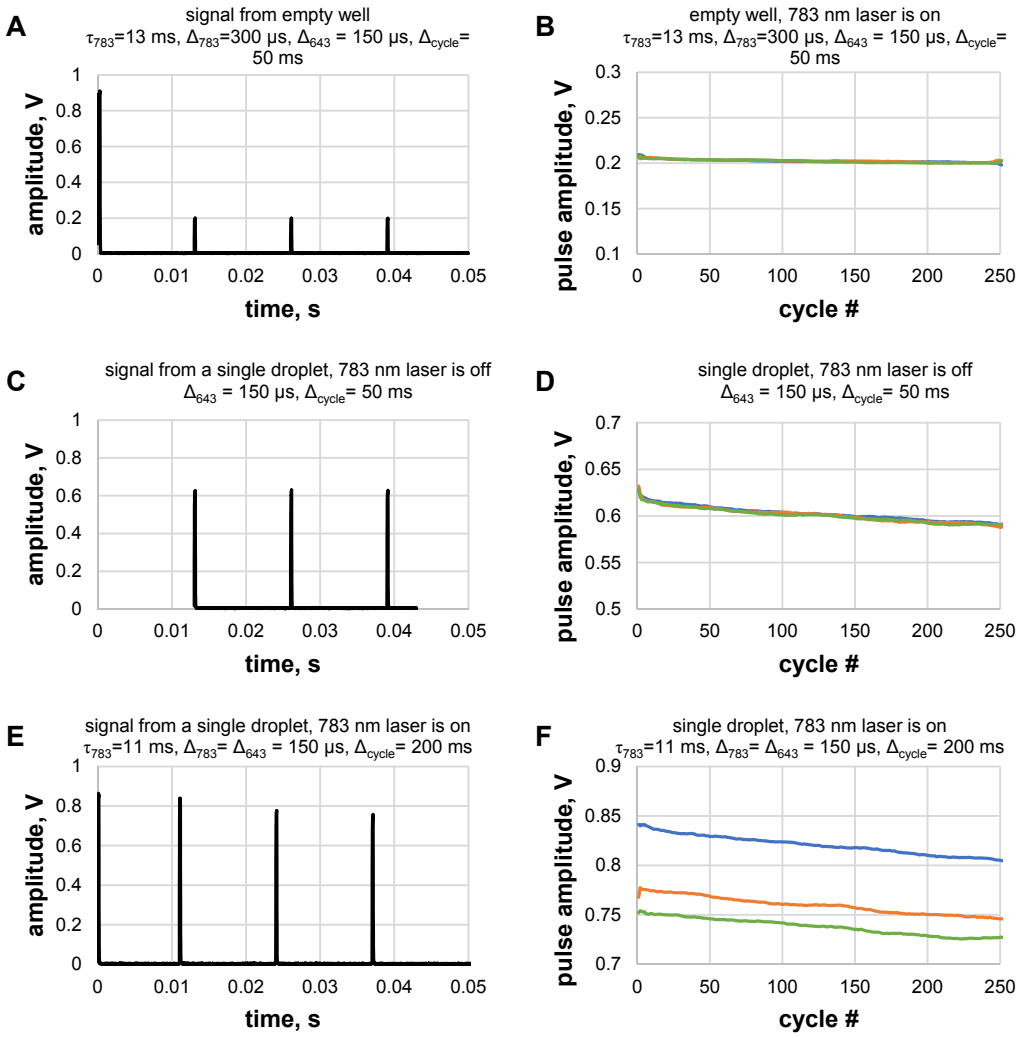

Raw pulsed signals (A, C, E) detected in single-point measurements and dependence of amplitude of the pulses on the number of switching cycle (B, D, F). (A, B) Signal from an empty well indicates background level. (C, D) Signal from a single droplet shows absence of switching, when the 783 nm laser is off. (E, F) Difference in amplitudes of the pulses indicates switching, when the 783 nm laser is on.

Figure S3. Dependence of photoswitching contrast on parameters of excitation/photoswitching laser pulses in experiment with a single droplet. 783 nm pulse irradiance was 4 kW/cm^2 and 643 nm laser pulses were 1.2 kW/cm^2.

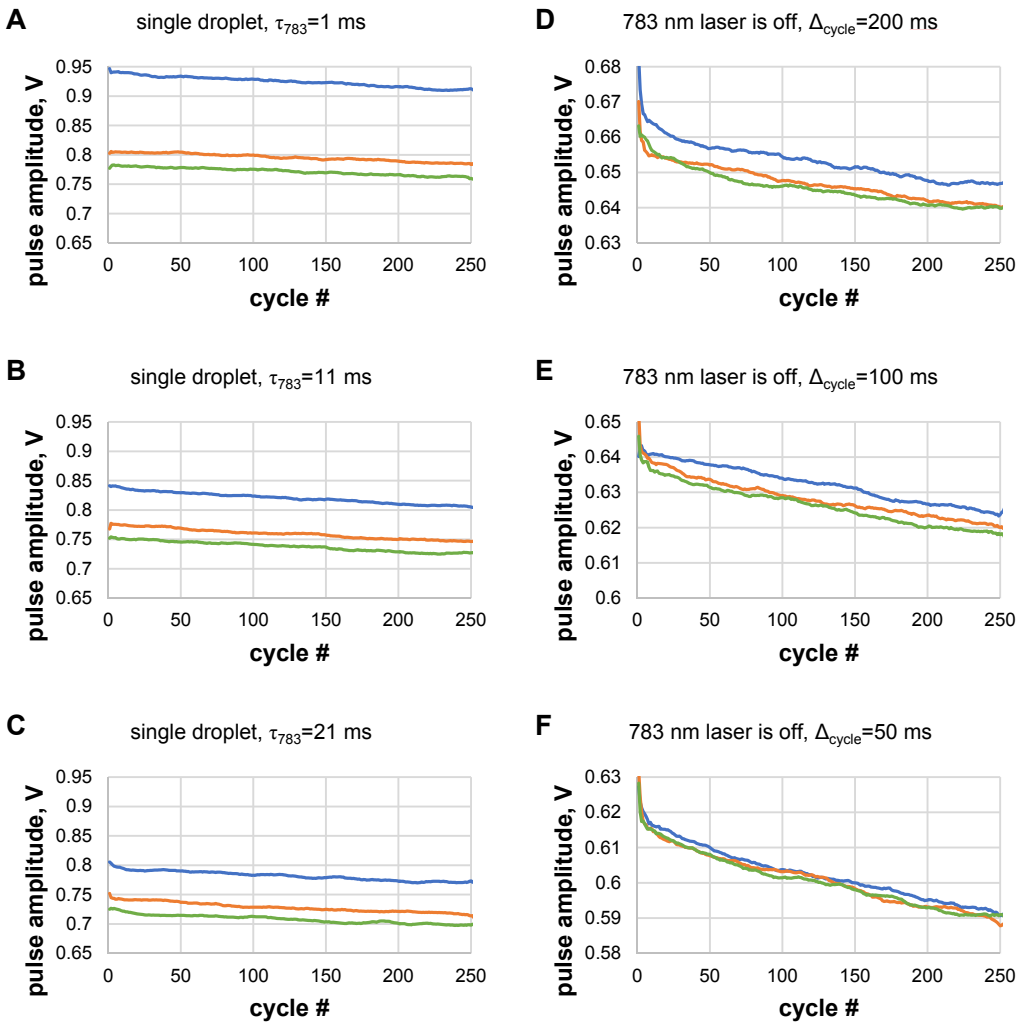

(A-C) Dependence of switching contrast on time delay τ_{NIR} between the 783 nm laser pulse and the 643 nm laser pulses: $\Delta_{783}=\Delta_{643}=150$ µs, $\Delta_{cycle}=200$ ms. (D-F) Dependence of uncontrollable transition of the protein into Pr form on the dwell-time between consecutive cycles: $\Delta_{643}=150$ µs.

Figure S4. Dependence of photoswitching contrast on parameters of excitation/photoswitching laser pulses in experiment with a single cell. 783 nm pulse irradiance was 4 kW/cm^2 and 643 nm laser pulses were 1.2 kW/cm^2.

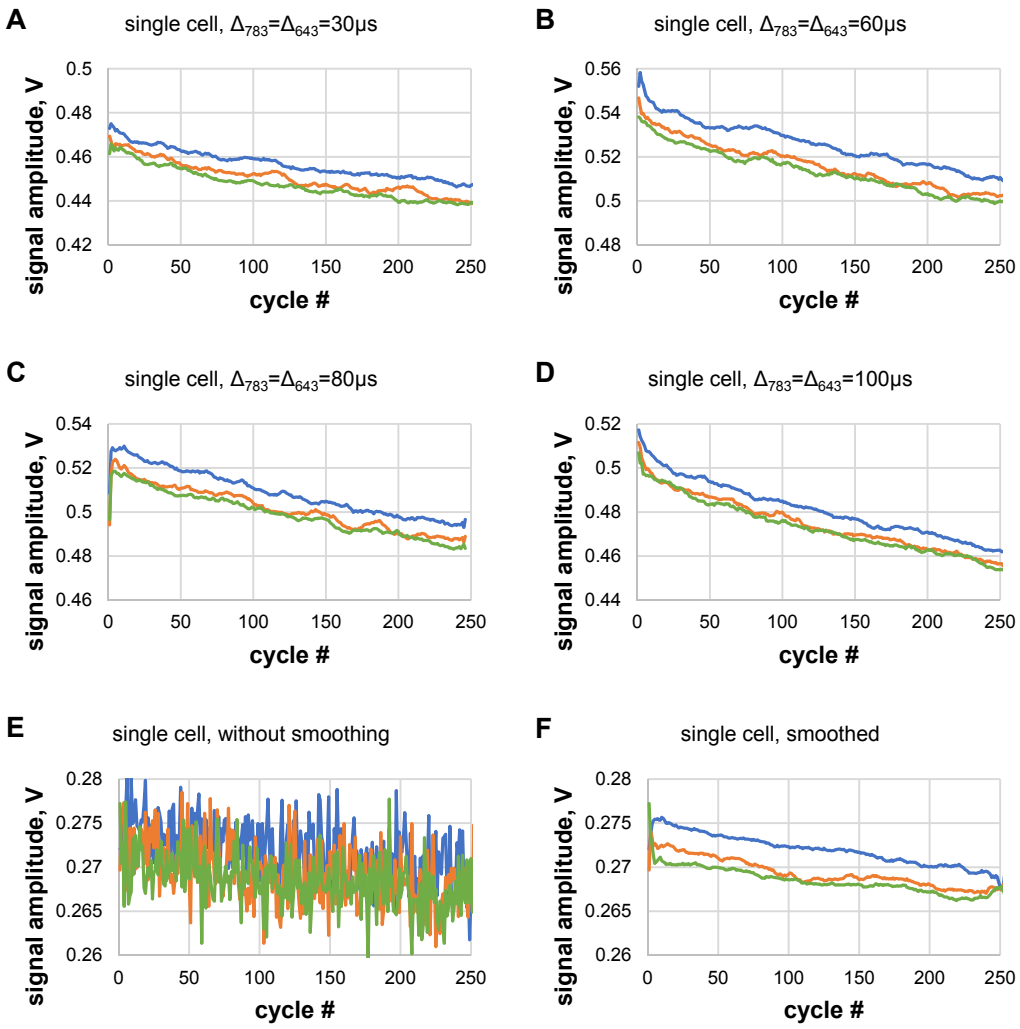

(A-D) Dependence of switching contrast on the energy of switching/excitation pulse: τ_{783}=1 ms, Δ_{cycle}=50 ms. Amount of energy depends on the pulse width Δ_{783} and Δ_{643}, while intensity is constant. Slow decrease in intensity indicates photobleaching, which is more expressed for higher energies/longer pulses, while switching contrast remains constant within 250 cycles. (E-F) Filtering of initial data recovered from the pulsed signal allows to observe switching in a cell.

Figure S5. In-flow measurements of constitutively fluorescent iRFP713 protein.

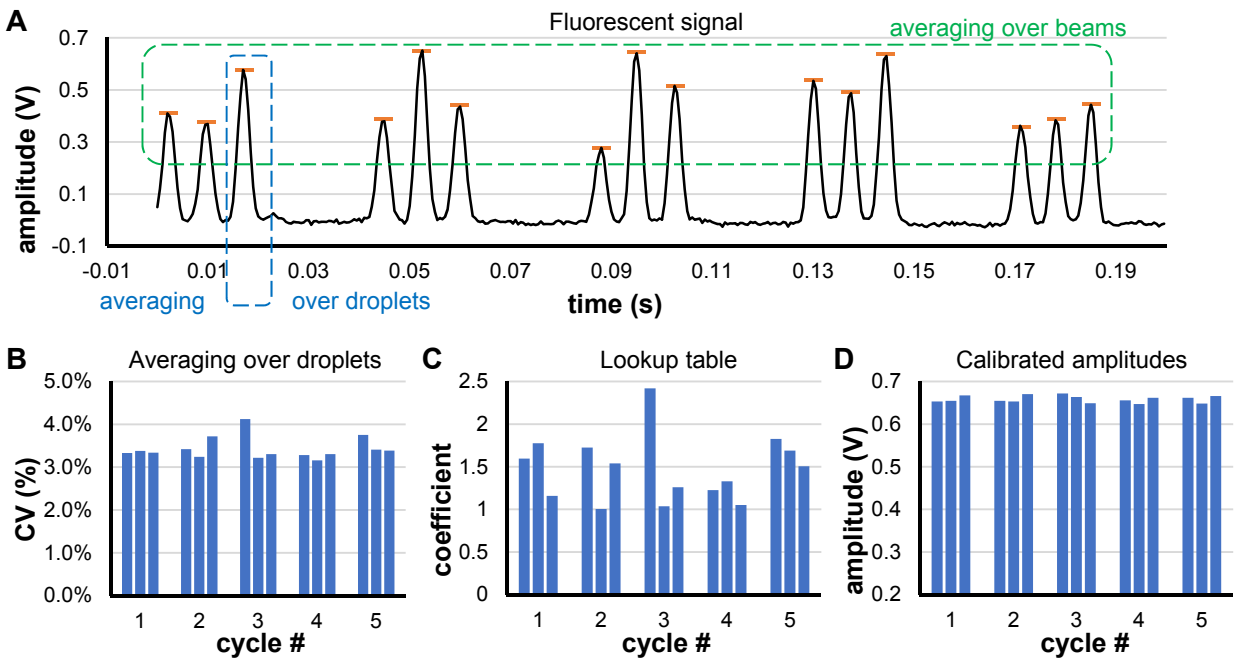

(A) Fluorescent signal (solid black line) and amplitudes of fluorescent pulses (red ticks) detected by processing software. (B) Droplet-to-droplet variation of amplitude for every pulse in the signal. (C) Array of calibration coefficients calculated using iRFP713. (D) Array of amplitudes of the fluorescent signal after calibration.

Figure S6. Photobleaching of constitutively fluorescent iRFP713 protein.

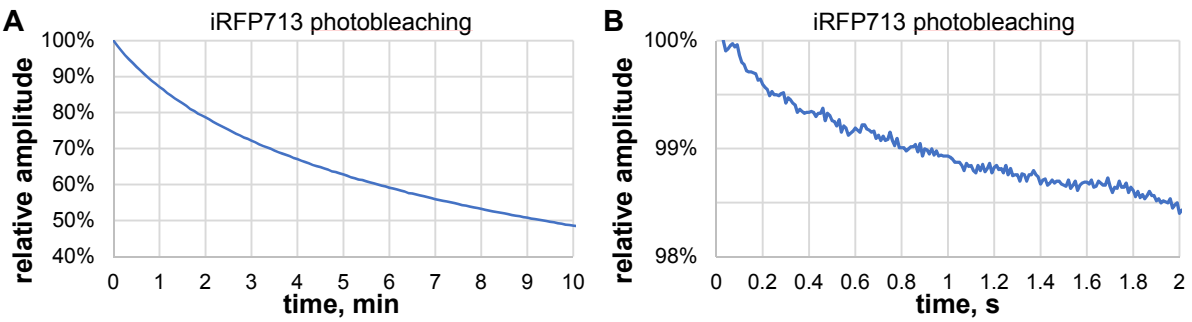

(A) Long-term and (B) short-term photobleaching of the purified iRFP713 solution are shown.

Figure S7. Dependence of switching contrast on brightness of droplets with different concentrations of DrBphP-PCM purified protein.

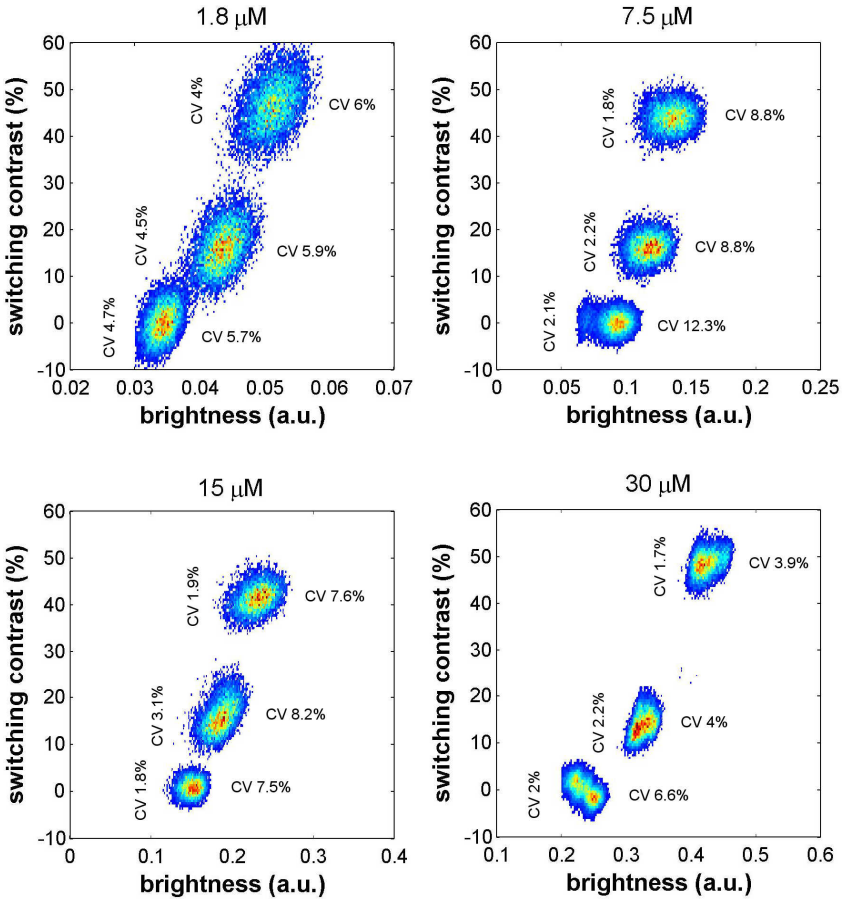

DrBphP-PCM protein concentrations (1.8 – 30 μM) are indicated at the top of the panels. The coefficients of variation (CVs) for the protein switching contrast and for the protein brightness are indicated at the left and right sides of the respective dotplots.